

A Tractable Model for Wirelessly Powered Networks with Energy Correlation

Na Deng, *Member, IEEE*, and Martin Haenggi, *Fellow, IEEE*

Abstract—In the analysis of large-scale wirelessly powered networks, the energy correlation is often ignored. While this leads to remarkably simple results for key performance metrics, it is typically not realistic and accurate. Considering the accuracy, tractability, and practicability tradeoffs, this paper introduces and promotes the Poisson disk process (PDP) as a model for the energized nodes that succeed in harvesting energy. To show that the model leads to analytically tractable results in several cases of interest, we derive its first and second moment densities, which fully characterize the PDP. Besides, we also provide tight bounds for its probability generating functional as well as its contact and nearest-neighbor distance distributions. Then, to show that the model is relevant for wirelessly powered networks—which all have positive energy correlation—we provide two approaches to fit the PDP to a given energized point process incorporating practical energy harvesting factors. Further, we derive the success probability in the information transmission phase, where the distribution of the active transmitters is modeled by a PDP. It turns out that the resulting PDP can closely model the distribution of actual energized nodes in terms of the success probability and other statistics while preserving analytical tractability.

Index Terms—Energy correlation; wirelessly powered networks; Poisson disk process; energized point process; stochastic geometry.

I. INTRODUCTION

A. Motivation

Radio frequency (RF) energy harvesting has quickly emerged as an attractive solution to energy-constrained wireless communication devices, especially the ones for which it is inefficient or even impractical to replace or recharge batteries [2, 3]. While the integration of RF energy harvesting with communication networks has many appealing advantages, it also adds an entirely new dimension to the performance analysis. The efficiency of energy transfer depends on the total received RF power rather than the signal-to-interference ratio (SIR) that is known as a strong indicator of the reliability of a communication link. Both the total received RF power and

the SIR depend on the network topology. Therefore, accurate modeling of the network topology in terms of both energy and information transfer becomes a key step towards a meaningful performance analysis of wirelessly powered networks.

Stochastic geometry has naturally been the preferred choice for modeling and analyzing wirelessly powered networks due to its realism in capturing the irregularity of node locations [4]. The existing research, however, is mostly based on the simplifying assumption that the active communication nodes form an independent thinning of the RF-powered nodes, which are independent of the RF power sources, see, e.g., [5–15]. As a result, the network topology in the energy transfer phase is independent of that in the communication phase. This clearly deviates from reality in wirelessly powered networks where the energy transfer performance has a fundamental impact on the topology of the energized RF-powered nodes (i.e., the active communication nodes) and hence the communication performance. This connection between the energy and information transfer fundamentally is a consequence of the spatial correlation of the amount of energy that can be harvested by RF-powered nodes, i.e., the energy correlation. In order to capture the energy correlation in wirelessly powered networks, a new point process, named *energized point process* (EPP), has recently been proposed to model the nodes that successfully harvest energy from the RF transmitters [16]. The EPP is a general model that can be concretized for any given energy harvesting scenario.

When applying the point processes to model a network, the accuracy and the tractability are two competing aspects that should be traded off. Generally, the more practical factors are considered, the less tractable the analysis. Despite the relevance of the EPP in modeling wirelessly powered networks with energy correlation, an exact characterization of the system performance indicators, such as the success probability and area spectral efficiency, is quite challenging. The approach taken in prior work is to use a homogeneous Poisson point process (PPP) or a Poisson cluster process (PCP) to approximate the EPP [16]. While this approach is reasonable, the PPP approximation is inaccurate beyond a specific range of system parameters, and the PCP approximation usually results in complex results involving multiple integrals. Thus, tractable models that accurately model wirelessly powered networks with energy correlation are still unavailable, which impedes the development of wireless energy transfer techniques. In this paper, we focus on the Poisson disk process (PDP) where disks are created around the RF transmitters modeled by a homogeneous PPP and only the RF-powered nodes located within such a disk are retained. The PDP is a simple type

Na Deng is with the School of Information and Communication Engineering, Dalian University of Technology (DLUT), Dalian, 116024, China, and also with the National Mobile Communications Research Laboratory, Southeast University, Nanjing, 210096, China (e-mail: dengna@dlut.edu.cn). Martin Haenggi is with the Dept. of Electrical Engineering, University of Notre Dame, Notre Dame 46556, USA (e-mail: mhaenggi@nd.edu).

Part of this work was presented at the 2020 IEEE International Communications Conference (ICC'2020) [1].

This work was supported by the National Natural Science Foundation of China under Grant 61701071, by the China Postdoctoral Science Foundation (2017M621129 and 2019T120204), by the open research fund of National Mobile Communications Research Laboratory, Southeast University (No. 2019D03), and by the Fundamental Research Funds for the Central Universities (DUT19RC(4)014).

of EPP where an RF-powered node succeeds in harvesting enough energy if and only if there is at least one RF transmitter within a given distance. As such, it achieves a good tradeoff between modeling accuracy and tractability and thus plays an important role in modeling, analyzing and designing future energy-limited scenarios such as wirelessly powered mobile networks and the Internet of Things.

B. Contributions

The contributions of the paper are:

- We introduce and promote the PDP as a model for wirelessly powered networks. The PDP not only captures the real network topology of wirelessly energized communications including the spatial correlation of energized nodes, but also is fairly tractable analytically, in contrast to other EPP models.
- We give closed-form expressions for the first- and second-order statistics of the PDP and show that the PDP is completely characterized by these two statistics. We also provide tight bounds on some additional fundamental statistics of the PDP, such as the probability generating functional (PGFL), the contact distribution function, and the nearest-neighbor distance distribution function.
- We propose two approaches to apply the PDP to model the network topology in the communication phase, for which the basic idea is to find a disk radius such that either the energy threshold (used to determine whether an RF-powered node is retained) or the density of the PDP is the same as the given EPP with practical energy harvesting factors.
- We analyze the information transmission success probability in a PDP-based network for two practical cases: (1) the desired transmitter is independent of the PDP (i.e., belongs to another system) and the interference comes from all the active RF-powered nodes; (2) the desired transmitter is a point of the PDP and the interference comes from the other active RF-powered nodes.
- We provide tight bounds as well as accurate approximations for the Laplace transform of the interference and the information transmission success probability in a PDP-based wirelessly powered network. To show the significant advantages of the proposed PDP over the existing approaches in capturing the energy correlation, we compare the analytical results with those in a practical EPP-based simulation as well as two approximations provided by a homogeneous PPP and a Matérn cluster process (MCP), respectively. We show that, remarkably, the PDP is superior to the PPP and the MCP in balancing the accurate modeling and analytical tractability.

C. Related Work

Stochastic geometry has been successfully applied to the performance analysis of wireless networks over the past two decades [17]. Recently, with research on wireless energy harvesting proliferating, point process models have found applications to wirelessly powered networks. The authors in [5] investigated the tradeoffs between transmit power and

density of mobile devices and wireless power beacons modeled as two independent homogeneous PPPs. As an extension, the work of [6] studied wireless energy harvesting in an uplink K -tier cellular network, where the locations of the users and base stations (BSs) were modeled using mutually independent PPPs. A similar setup was considered in [7] with focus on the downlink analysis. The work of [8] introduced and analyzed the energy meta distribution, which is the distribution of the conditional energy outage probability given the point process. This new metric provides much more fine-grained information than the mean that is usually considered. Moreover, analytical results on wireless energy harvesting were also obtained for relay [9], cognitive [10, 11], device-to-device [12], millimeter-wave [13, 14] and sensor [15] networks using PPP-based models. Although relatively sparse, there has been another line of research considering the setups where either the RF-powered nodes or the RF power sources are modeled by a non-Poisson point process, such as the Ginibre point process in [18, 19], the Poisson hole process in [20] and the PCP in [21, 22]. To maintain analytical tractability, the influence of the energy transfer performance on the network topology of the communication nodes is mostly simplified to an independent thinning of the original point process of the RF-powered nodes, with the thinning probability taken to be the average energy harvesting success probability. As a result, the inherent correlation between the energy and information transfer phases, namely the energy correlation, is ignored. More importantly, subsequent impacts of the energy correlation on the communication performance are also masked.

Since the energy correlation is a differentiating feature in wirelessly powered systems, it is crucial and intriguing to accurately incorporate it into the wireless-powered network performance analysis. Thus motivated, we introduced the energized point process (EPP), a new point process that captures the critical influence of the random field of harvested energy on the spatial distribution of active RF-powered nodes [16]. It is a general model, or, rather, a general concept for characterizing the spatial configuration of the nodes that successfully harvest energy from the RF transmitters. In [16], we concretized the EPP by focusing on the energy harvesting from a Poisson field of RF power sources and considering two energy harvesting models with different degrees of practicality. However, due to the absence of an analytical form for the PGFL and the Palm measure of the EPP, an exact characterization of the communication performance such as the information transmission success probability is an unsurmountable problem. Thus, we turned to approximating the EPP by a homogeneous PPP with the same density and a PCP by matching the first- and second-order statistics. However, the PPP approximation causes inaccuracies while the PCP approximation leads to significantly increased complexity in the performance evaluation. In contrast, this paper addresses the tradeoff between accurate modeling and tractable performance analysis by introducing a relatively simple EPP, namely the PDP, which can match a given EPP by suitably adjusting the disk radius. It corresponds to a simplified energy harvesting model where successful energy harvesting occurs if an RF power source is located within a certain

distance. We derive tight upper and lower bounds for the PGFL and its Palm version for the PDP, which makes it possible to give analytical expressions for the information transmission success probability of a wirelessly powered network with energy correlation.

D. Mathematical Preliminaries

Here we give a brief overview of some terminology and mathematical tools from stochastic geometry. Readers are referred to [17, 23, 24] for further details.

Definition 1 (Germ-grain model [17, Def. 13.1]). Let $\Phi = \{x_1, x_2, \dots\}$ be a point process on \mathbb{R}^2 , the germs, and (S_1, S_2, \dots) a collection of random non-empty sets, the grains. Then the union $\Xi = \bigcup_{i \in \mathbb{N}} x_i + S_i$ is a germ-grain model.

Definition 2 (Boolean model [17, Def. 13.4]). A Boolean model is a germ-grain model where the germ point process is a uniform PPP and the grains S_i are i.i.d.

Definition 3 (Boolean Cox process on disks [23, Sec. 2.1]). Let $\Xi = \bigcup_{i \in \mathbb{N}} b(y_i, R)$ be a Boolean model where $b(y_i, R)$ denotes a disk centered at y_i with radius R , i.e., $S_i = b(o, R)$ for $\forall i \in \mathbb{N}$. Then, the Boolean Cox process on disks is a Cox process with random driving measure Λ induced by Ξ as

$$\Lambda(dx) = \begin{cases} \lambda_I dx & \text{if } x \in \Xi \\ \lambda_{II} dx & \text{if } x \notin \Xi, \end{cases} \quad (1)$$

where $0 \leq \lambda_I, \lambda_{II} < \infty$ and $\max\{\lambda_I, \lambda_{II}\} > 0$.

Note that when $\lambda_I = 0$, it reduces to the Swiss cheese model (also called Poisson hole process); and when $\lambda_{II} = 0$, it reduces to the inner-city model [17]. The former has been used in cognitive networks [25], heterogeneous cellular networks [26], etc., to characterize the repulsion among wireless nodes, while the literature on the latter (called the PDP in this paper) mostly focuses on the spatial characteristics of the point process [23, 24] rather than the communication performance in wireless networks.

Definition 4 (Matérn cluster process [17, Def. 3.6]). The Matérn cluster process is a Poisson cluster process, where the parent point process is a PPP with density λ . The points in each cluster are placed uniformly at random in a disk of radius D around their parent points and the number of points in each cluster follows a Poisson distribution with mean \bar{c} .

The MCP is also a Cox process with random driving measure $\Lambda_{\text{MCP}}(dx) = \kappa_{\text{MCP}}(x)dx$, where the intensity field $\kappa_{\text{MCP}}(x) = \lambda_I \Phi_1(b(x, D))$ and $\lambda_I = \bar{c}/(\pi D^2)$.

E. Organization

The rest of the paper is organized as follows. Section II describes the system model and applies the PDP to a wirelessly powered network. Section III gives the fundamental properties of the PDP. Section IV details the information transmission phase, which covers the analysis of the communication performance in a PDP-model network and two approximations provided by a homogeneous PPP as well as an MCP. Section

V presents the results and the advantages of the PDP over the PPP and MCP, and Section VI offers the concluding remarks.

II. SYSTEM MODEL

In this section, we consider a wirelessly powered communication network, where the locations of RF transmitters and RF-powered nodes follow two independent Poisson point processes. As discussed above, there is spatial correlation among the amount of harvested energy by RF-powered nodes. We first formally define the EPP, which is formed by the RF-powered nodes that succeed in harvesting enough energy for subsequent transmission and then establish the key relationship between the PDP and the EPP in order to use the PDP as a model for the wirelessly powered network.

A. Energized Point Process

Definition 5 (Energized point process [16]). Let Φ_f and Φ_d be two point processes of RF transmitters and RF-powered nodes, respectively. Then the energized point process Φ_e is defined as a dependent thinning of Φ_d as

$$\Phi_e \triangleq \{x \in \Phi_d : E(x, \Phi_f) = 1\}, \quad (2)$$

where $E(x, \Phi_f) \in \{0, 1\}$ is the energy indicator function describing whether enough energy can be harvested from Φ_f at location x .

Definition 5 stipulates that an RF-powered node becomes active if and only if it harvests enough energy in the energy transfer phase. Note that in this definition, Φ_f and Φ_d can be arbitrary point processes. In this paper, the two point processes Φ_f and Φ_d are assumed to be two independent homogeneous PPPs with densities λ_f and λ_d , respectively. Then the energy indicator function is

$$E(x, \Phi_f) = \mathbf{1}(\varepsilon(x, \Phi_f) > \xi), \quad (3)$$

where $\varepsilon(x, \Phi_f)$ denotes the energy harvested from Φ_f at location x and ξ is the energy threshold.

In addition to the spatial configuration, the amount of energy harvested also depends strongly on the propagation loss experienced by the RF signals. It is assumed that the RF signals merely experience large-scale path loss, and a linear energy harvesting model is adopted¹. Hence, the harvested energy at x is the aggregate received signal strength from all the RF transmitters in Φ_f , which is given by

$$\varepsilon(x, \Phi_f) = \sum_{y \in \Phi_f} \ell(y - x), \quad (4)$$

where $\ell(x) \triangleq \|x\|^{-\alpha}$ is the path loss function with exponent α for the energy transfer.

¹The results for other (non-linear) energy harvesting models can be obtained similarly. If the actual harvested energy is a non-linear function f of ε , where f is assumed strictly monotonically increasing, then ξ in (3) merely needs to be replaced by $f^{-1}(\xi)$ to capture the non-linearity.

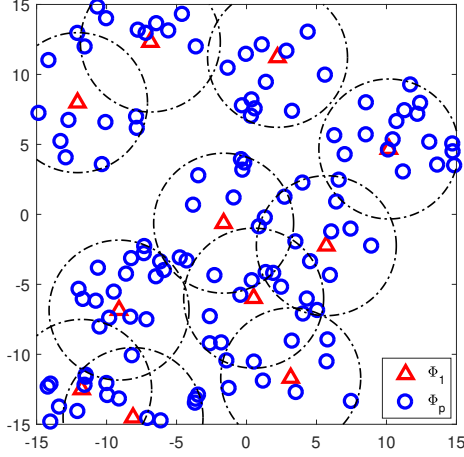


Fig. 1. A realization of the PDP with $\beta = 0.01$, $\lambda_I = 0.2$, and $R = 5$.

B. PDP Model for EPP

Definition 6 (Poisson disk process, PDP). *The Poisson disk process is a Boolean Cox process on disks with $\lambda_{II} = 0$.*

Figure 1 shows an example realization of the PDP. From the definition, the PDP Φ_p can be described by a Boolean model on disks $\Xi = \bigcup_{y \in \Phi_1} b(y, R)$ with two PPPs Φ_1 and Φ_2 of densities β and λ_I , respectively. Hence we have $\Phi_p = \Phi_2 \cap \Xi$. Interestingly, there are some similarities between a PDP and a MCP: (1) they are both derived from the PPP; and (2) the grains in the PDP and the clusters in the MCP are both disks. The key difference is that in the MCP, the conditional density at a location is given by the number of times it is covered by a disk instead of being just binary as in the PDP. The PDP is a dependent thinning of Φ_2 and, from Definition 3, its random intensity field $\kappa_p(x) = \lambda_I \mathbf{1}(\Phi_1(b(x, R)) > 0)$, where $\mathbf{1}(\cdot)$ denotes the indicator function and $\Phi_1(b(x, R))$ is the number of points in Φ_1 located in $b(x, R)$.

Compare Definitions 6 and 5 and let Φ_1 be Φ_f , β be λ_f , Φ_2 be Φ_d , and λ_I be λ_d . It is easily seen that the PDP behaves like an EPP but has a simpler structure. Thus, it is intuitive to use the PDP as a tractable model for the active RF-powered nodes by establishing a relationship between the PDP model and a given EPP that incorporates practical energy harvesting factors. The basic idea is to find an equivalent disk radius R such that the mechanism of retaining points in the PDP mimics that in the EPP as closely as possible, or, equivalently, to find how to capture the condition $\varepsilon(x, \Phi_f) > \xi$ by $\Phi_f(b(x, R)) > 0$ for $x \in \Phi_d$.

We provide two different approaches to relate Φ_e and Φ_p :

- **Approach I:** The first approach is to set $R = \xi^{-1/\alpha}$, based on the fact that $\Phi_f(b(x, R)) > 0$ is a sufficient condition for $\varepsilon(x, \Phi_f) > \xi$. Thus, we have $\Phi_p \subset \Phi_e$ and $\lambda_p < \lambda_e$.
- **Approach II:** The second approach is to determine R by setting $\mathbb{P}(\Phi_f(b(x, R)) > 0) = \mathbb{P}(\varepsilon(x, \Phi_f) > \xi)$ such that $\lambda_p = \lambda_e$.

Due to the motion-invariance of Φ_p , $\mathbb{P}(\varepsilon(x, \Phi_f) > \xi) =$

$\mathbb{P}(\varepsilon(o, \Phi_f) > \xi) \triangleq P_e$ is the energy harvesting success probability of the RF-powered node at the origin. Let $\varphi(w) \triangleq \mathbb{E}(e^{jw\varepsilon(o, \Phi_f)})$ be the characteristic function of the harvested energy at the origin. According to [17, Sec. 5.15], the characteristic function for $\alpha > 2$ is expressed as

$$\varphi(w) = \exp(-\lambda_f \pi \Gamma(1 - \delta) w^\delta e^{-j\pi\delta/2}), \quad w \geq 0, \quad (5)$$

where $j = \sqrt{-1}$ and $\delta = 2/\alpha$. Using the Gil-Pelaez theorem [27], we have

$$\begin{aligned} P_e &= \frac{1}{2} + \frac{1}{\pi} \int_0^\infty \frac{\Im(e^{-jw\xi} \varphi(w))}{w} dw \\ &= \frac{1}{2} + \frac{1}{\pi} \int_0^\infty \frac{e^{-\lambda_f \pi \Gamma(1 - \delta) w^\delta \cos(\delta\pi/2)} \sin(\lambda_f \pi \Gamma(1 - \delta) w^\delta \sin(\delta\pi/2) - w\xi)}{w} dw. \end{aligned} \quad (6)$$

Then, according to (12) and $\mathbb{P}(\Phi_f(b(o, R)) > 0) = P_e$, we have

$$R = \sqrt{\frac{1}{\pi \lambda_f} \ln \frac{1}{1 - P_e}}. \quad (7)$$

When $\alpha = 4$, we have

$$\varphi(w) = \exp(-\lambda_f \pi^{3/2} \sqrt{w} e^{-j\pi/4}), \quad w \geq 0, \quad (8)$$

and in this case the energy harvesting success probability admits the closed-form expression

$$P_e = 1 - \frac{1}{\sqrt{\pi}} \Gamma\left(\frac{1}{2}, \frac{\pi^3 \lambda_f^2}{4\xi}\right). \quad (9)$$

Remark 1: When $\alpha \rightarrow \infty$, we have $\ell(x) \rightarrow 0$ for $\|x\| > 1$ and $\ell(x) \rightarrow \infty$ for $\|x\| < 1$. For the EPP in this case, only those points with a distance to the RF transmitters smaller than 1 can be energized. As a result, the EPP converges to the PDP with $R = 1$. This observation further justifies the use of the PDP to characterize the EPP.

Figure 2 shows a comparison between the realizations of the EPP and the Approach II-based PDP under the same realization of Φ_f and Φ_d . It is observed that the points retained in the EPP are almost the same as those retained in the PDP, which demonstrates the good match between the two point processes. The accuracy of the match is evaluated by comparing the first- and second-order statistics in Section V, where it is shown that Approach II is better than Approach I in terms of the accuracy of modeling the given EPP. Hence, in the following analysis, we will use the Approach II-based PDP to model the active RF-powered nodes in the communication phase.

C. Communication Model

Each energized RF-powered node is assumed to have a dedicated receiver at distance d in a random orientation. Hence, the energized RF-powered nodes and their receivers form a PDP bipolar network. The transmit power of RF-powered nodes is assumed to be one. We further assume that the path loss model is the same as in the energy transfer phase and all power fading coefficients are i.i.d. exponential (Rayleigh fading) with mean one. For the information transmission phase, the

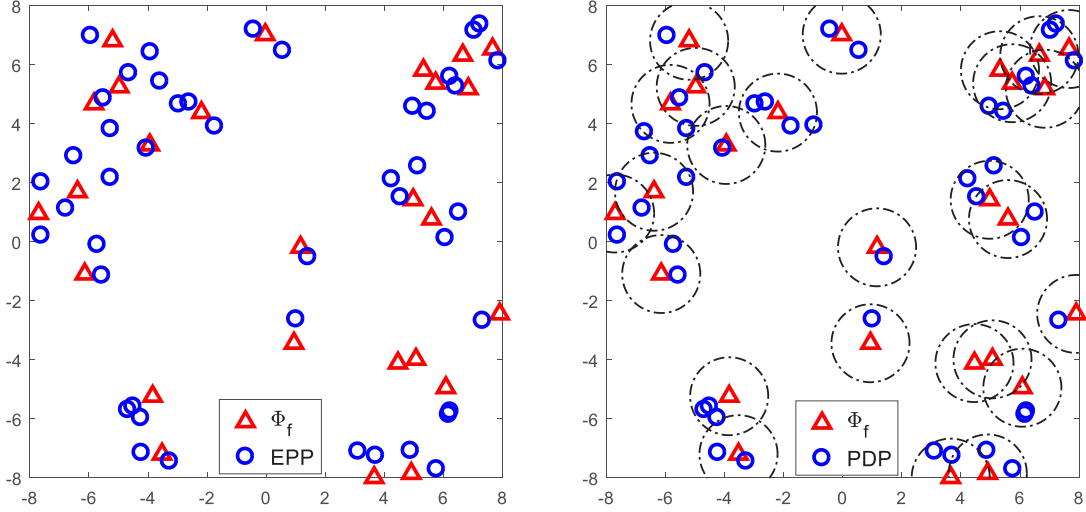


Fig. 2. Comparison of the EPP (left) and the Approach II-based PDP (right) with $\lambda_f = 0.1$, $\lambda_d = 1$, $\xi = 0.5$, and $\alpha = 4$, where $R = 1.32$ in the PDP.

received SIR is a strong indicator of the performance of a wireless link, the distribution of which (i.e., the transmission success probability) depends on the joint distribution of the received powers from the serving node and the interfering nodes. Depending on whether the desired transmitter belongs to the PDP, we consider two types of practical scenarios:

- **Type I:** This case considers the SIR distribution in a PDP field of interferers, i.e., the desired transmitter does not belong to the PDP². Without loss of generality, due to the stationarity of the PDP, the typical receiver is assumed to be located at the origin and its corresponding transmitter at $z = (d, 0)$. Then the received SIR of the typical receiver is given by

$$\text{SIR} = \frac{\ell(z)h_{zo}}{\sum_{x \in \Phi_p} \ell(x)h_{xo}}, \quad (10)$$

where h_{xy} denotes power fading coefficient between node x and y , and the interference is $I \triangleq \sum_{x \in \Phi_p} \ell(x)h_{xo}$.

- **Type II:** This case considers the SIR distribution where the desired transmitter belongs to the PDP. Since the PDP is a stationary point process, we condition on that the typical transmitter (active RF-powered node) is located at the origin, with the corresponding typical receiver at $z = (d, 0)$. Letting $\Phi_p^o \triangleq (\Phi_p \mid o \in \Phi_p)$ and $\Phi_p^{!o} \triangleq \Phi_p^o \setminus \{o\}$, the received SIR of the typical receiver is given by

$$\text{SIR} = \frac{\ell(z)h_{oz}}{\sum_{x \in \Phi_p^{!o}} \ell(x-z)h_{xz}}. \quad (11)$$

In this case, the interference is $I^!(z) \triangleq \sum_{x \in \Phi_p^{!o}} \ell(x-z)h_{xz}$.

In the next section, we will provide some of the pertinent properties of the PDP, in particular, the PGFL, to facilitate the performance analysis in wirelessly powered networks modeled by the PDP.

²This case is usually used to characterize the interference from the energized RF-powered nodes to other systems, e.g., a cellular link can be interfered by all energized D2D links if they share the same frequency band.

III. FUNDAMENTALS OF THE POISSON DISK PROCESS

A. Basic Properties

Since Φ_p is motion-invariant, its density is a constant and its second moment density $\rho^{(2)}(x, y)$ depends only on the distance $\|x - y\|$. Hence there is a density $\rho_{\text{mi}}^{(2)}$ such that $\rho_{\text{mi}}^{(2)}(\|x - y\|) \equiv \rho^{(2)}(x, y)$. The density of the PDP is $\lambda_p = \lambda_I P_p(R)$, where

$$P_p(R) = 1 - \exp(-\beta\pi R^2) \quad (12)$$

is the retention probability of the typical point of Φ_2 [23]. The second moment density is a key statistic that describes the pairwise correlation of a point process. For the PPP, $\rho_{\text{mi}}^{(2)} = \lambda^2$, because points are independent. If $\rho_{\text{mi}}^{(2)}(r) > \lambda^2$, points at distance r exhibit clustering, and if $\rho_{\text{mi}}^{(2)}(r) < \lambda^2$, points at distance r exhibit repulsion. In the following lemma, we give a closed-form expression for the second moment density of the PDP.

Lemma 1. *The second moment density of the PDP is*

$$\rho_{\text{mi}}^{(2)}(u) = \lambda_I^2 \left(1 - 2e^{-\beta\pi R^2} + e^{-\beta(2\pi R^2 - A(R, u))} \right), \quad (13)$$

where

$$A(R, u) = \begin{cases} 2R^2 \arccos\left(\frac{u}{2R}\right) - u\sqrt{R^2 - \frac{u^2}{4}} & \text{if } u \leq 2R \\ 0 & \text{otherwise} \end{cases} \quad (14)$$

is the intersection area of two disks with radius R at distance u .

Proof: See Appendix A

The pair correlation function (pcf) is given by [17, Def. 6.6]

$$\begin{aligned} g_p(u) &\triangleq \frac{\rho_{\text{mi}}^{(2)}(u)}{\lambda_p^2} \\ &= 1 + \frac{e^{-2\beta\pi R^2} (e^{\beta A(R, u)} - 1)}{(1 - e^{-\beta\pi R^2})^2}. \end{aligned} \quad (15)$$

As expected from the clustered nature of the PDP, $g_p(u) \geq 1$ for all $u \geq 0$. Given the density λ_p and the pair correlation function $g_p(u)$, we obtain for the PDP that

$$R = \frac{1}{2} \min_{u>0} \{u: g_p(u) = 1\}, \quad (16)$$

$$\beta = \frac{1}{\pi R^2} \log \frac{g_p(0)}{g_p(0) - 1}, \quad (17)$$

$$\lambda_I = \lambda_p / g_p(0). \quad (18)$$

Thus, the PDP is fully characterized by its first-order statistic λ_p and its second-order statistic $g_p(u)$ (or $\rho_{\text{mi}}^{(2)}(u)$)³. This implies that a suitable PDP can be used to generate point distributions with any given intensity and pcf for which $g_p(u) \geq 1 \forall u \geq 0$. In other words, once the first- and second-order statistics of an actual network, where ‘‘attraction’’ exists between transmitters, are given or obtained numerically, we can use the PDP to model this network.

B. Probability Generating Functional

For a point process Φ , the PGFL is defined as [17, Def. 4.3]

$$\mathcal{G}[v] \triangleq \mathbb{E} \left(\prod_{x \in \Phi} v(x) \right), \quad (19)$$

where $v: \mathbb{R}^2 \mapsto [0, 1]$ such that $1 - v$ has bounded support. Since PDP is obtained by a dependent thinning of the PPP, it is difficult to derive the exact PGFL. Instead, we provide upper and lower bounds on its PGFL in the following theorem. For notational convenience, we define

$$\begin{aligned} y_0 &\triangleq \arg \min \{y \in \Phi_1: \|y\|\}, \\ b^c(o, t) &\triangleq \mathbb{R}^2 \setminus b(o, t), \\ V(R, y) &\triangleq \int_{b(y, R)} [1 - v(x)] dx. \end{aligned}$$

Theorem 1 (Bounds on the PGFL of the PDP). *Let*

$$\hat{\mathcal{G}}[v] \triangleq \beta \int_{\mathbb{R}^2} e^{-\beta\pi\|y\|^2 - \lambda_I V(R, y)} dy, \quad (20)$$

$$\check{\mathcal{G}}[v] \triangleq \exp \left(-\beta \int_{\mathbb{R}^2} [1 - e^{-\lambda_I V(R, y)}] dy \right). \quad (21)$$

The PGFL for the PDP is bounded by $\check{\mathcal{G}}[v] < \mathcal{G}[v] < \hat{\mathcal{G}}[v]$.

Proof: See Appendix B.

The PGFL is a key tool in point process theory that has many applications in wireless networks. Most notably, it can be used to evaluate the Laplace transform of the sum of all the interfering signal powers emitted from a PDP field of interferers. We also consider the conditional PGFL conditioning on a point of the process Φ_p being at the origin but without including the point. Denoting by $\mathbb{E}^{!o}(\cdot)$ the expectation with respect to the reduced Palm measure [17, Def. 8.4.1], the conditional PGFL is defined as

$$\mathcal{G}^![v] \triangleq \mathbb{E}^{!o} \left(\prod_{x \in \Phi_p} v(x) \right). \quad (22)$$

Next, we derive bounds and an approximation for the conditional PGFL.

³The MCP also has this property but not the Thomas cluster process.

Theorem 2 (Bounds on the conditional PGFL of the PDP).

Let

$$\hat{\mathcal{G}}^![v] \triangleq \frac{1}{P_p(R)} \int_{b(o, R)} \beta e^{-\beta\pi\|y\|^2 - \lambda_I V(R, y)} dy, \quad (23)$$

$$\begin{aligned} \check{\mathcal{G}}^![v] &\triangleq \frac{1}{P_p(R)} \int_{b(o, R)} \beta e^{-\beta\pi\|x\|^2 - \lambda_I V(R, x)} \\ &\times \exp \left(-\beta \int_{b^c(o, \|x\|)} 1 - e^{-\lambda_I V(R, y)} dy \right) dx. \end{aligned} \quad (24)$$

The conditional PGFL of the PDP is bounded by $\check{\mathcal{G}}^![v] < \mathcal{G}^![v] < \hat{\mathcal{G}}^![v]$.

Proof: See Appendix C.

Since $b^c(o, R) \subset b^c(o, \|x\|)$ if $x \in b(o, R)$, the lower bound $\check{\mathcal{G}}^![v]$ with three nested integrals can be used to obtain an approximation in a simpler form (two nested integrals) as

$$\begin{aligned} \check{\mathcal{G}}^![v] &\approx \frac{1}{P_p(R)} \exp \left(-\beta \int_{b^c(o, R)} 1 - e^{-\lambda_I V(R, y)} dy \right) \\ &\times \int_{b(o, R)} \beta e^{-\beta\pi\|y\|^2 - \lambda_I V(R, y)} dy. \end{aligned} \quad (25)$$

Remark 2: To maintain tractability, the overlaps of the disks in the Boolean model are not considered in deriving the lower bounds in Theorems 1 and 2. Hence, the points located in the overlaps will be repeatedly considered in calculating the lower bound of the PGFL. As a consequence, the tightness of the lower bounds depends on the number of disks that cause a point to be retained due to the overlaps in the Boolean model, which follows a Poisson distribution with mean $\beta\pi R^2$ [17, Thm. 13.5]. This also indicates that the tightness of the lower bounds is agnostic to Φ_2 . Denoting by P_c the probability that the typical point is covered by less than two disks, we have $P_c = e^{-\beta\pi R^2} (1 + \beta\pi R^2)$. Then, when $P_c \rightarrow 1$, i.e., $\beta\pi R^2 \rightarrow 0$, the lower bounds get tight.

Remark 3: The tightness of the upper bounds is mainly determined by the monotonicity of $v(x)$ with $\|x\|$ and the number of points of Φ_2 in the closest disk, since only the closest disk to the origin in the Boolean model is considered, thereby neglecting the effect of the distant points in the PDP. When $v(x)$ is monotonically decreasing with $\|x\|$, e.g., when using it to represent path loss, the upper bounds are also rather tight. Moreover, denoting by P_n the probability that there is no point of Φ_2 located in the closest disk, we have $P_n = e^{-\lambda_I \pi R^2}$. The higher the probability P_n , the more likely the upper bounds deviate from the exact results. When $\lambda_I \rightarrow 0$ or $R \rightarrow 0$, $P_n \rightarrow 1$. In this case, there is almost no point in the PDP. But, obviously, this is a rather unrealistic situation. That is to say, for a wide variety of scenarios (where parameters like λ_I and R are seldom set very small), the above upper bounds are quite tight.

From the discussions above, we conclude that both the upper and lower bounds are very tight for scenarios with small β and large λ_I . More details on the tightness are provided in the numerical results section.

C. Important Distances

1) *Contact distribution function:* The contact distance at location u of a point process Φ is $\|u - \Phi\|$, and the contact

distribution function or empty space function F^u is the cumulative distribution function (cdf) of $\|u - \Phi\|$ [17, Def. 2.38]:

$$F^u(r) \triangleq \mathbb{P}(\|u - \Phi\| \leq r) = \mathbb{P}(\Phi(b(u, r)) > 0). \quad (26)$$

If Φ is stationary, F^u does not depend on the location u and is given by $F(r) = \mathbb{P}(\Phi(b(o, r)) > 0)$. Upper and lower bounds on the cdf of the contact distance for the PDP are derived next.

Theorem 3. *Let*

$$\hat{F}(r) \triangleq 1 - \exp\left(-2\pi\beta \int_0^\infty (1 - e^{-\lambda_I \tilde{A}(R, r, t)}) dt\right), \quad (27)$$

$$\check{F}(r) \triangleq 1 - \int_0^\infty 2\pi\beta t e^{-\beta\pi t^2 - \lambda_I \tilde{A}(R, r, t)} dt, \quad (28)$$

where

$$\tilde{A}(R, r, t) = \begin{cases} \pi(\min\{r, R\})^2, & t \leq |R - r| \\ R^2\varphi_R + r^2\varphi_r - \chi(R, r, t), & |R - r| < t < R + r \\ 0, & \text{otherwise} \end{cases} \quad (29)$$

is the intersection area of two disks with radii R and r at distance t ,

$$\begin{aligned} \varphi_R &= \arccos\left(\frac{R^2 + t^2 - r^2}{2Rt}\right), \\ \varphi_r &= \arccos\left(\frac{r^2 + t^2 - R^2}{2rt}\right), \\ \chi(R, r, t) &= 2\sqrt{p(p-R)(p-r)(p-t)}, \end{aligned}$$

and $p = (R + r + t)/2$. Then, the cdf of the contact distance for the PDP is bounded by $\check{F}(r) < F(r) < \hat{F}(r)$.

Proof: According to (26), the contact distribution function of Φ_p is expressed as

$$\begin{aligned} F(r) &= 1 - \mathbb{P}(\Phi_p(b(o, r)) = 0) \\ &= 1 - \mathbb{E}\left(\prod_{x \in \Phi_p} [1 - \mathbf{1}(\|x\| \leq r)]\right) \\ &= 1 - \mathcal{G}[1 - \mathbf{1}(\|x\| \leq r)]. \end{aligned} \quad (30)$$

Following the results in Theorem 1, the upper and lower bounds of the contact distribution function are obtained. Specifically, the upper bound is given by

$$\begin{aligned} F(r) &< 1 - \check{\mathcal{G}}[1 - \mathbf{1}(\|x\| < r)] \\ &= 1 - \exp\left(-\beta \int_{\mathbb{R}^2} 1 - \exp\left(-\lambda_I \int_{b(y, R)} \mathbf{1}(\|x\| \leq r) dx\right) dy\right) \\ &\stackrel{(a)}{=} 1 - \exp\left(-2\pi\beta \int_0^\infty (1 - e^{-\lambda_I \tilde{A}(R, r, t)}) t dt\right), \end{aligned} \quad (31)$$

and the lower bound is given by

$$\begin{aligned} F(r) &> 1 - \hat{\mathcal{G}}[1 - \mathbf{1}(\|x\| < r)] \\ &= 1 - \beta \int_{\mathbb{R}^2} e^{-\beta\pi\|y\|^2 - \lambda_I \int_{b(y, r)} \mathbf{1}(\|x\| \leq r) dx} dy \\ &\stackrel{(b)}{=} 1 - \int_0^\infty 2\pi\beta t e^{-\beta\pi t^2 - \lambda_I \tilde{A}(R, r, t)} dt, \end{aligned} \quad (32)$$

where steps (a) and (b) are derived using polar coordinates and $\int_{b(y, R)} \mathbf{1}(\|x\| \leq r) dx$ which is the area of the overlap between $b(o, r)$ and $b(y, R)$. ■

2) *Nearest-neighbor distance distribution function:* The nearest-neighbor distance is the distance from a point $x \in \Phi$ to its nearest neighbor, given by $\|x - \Phi \setminus \{x\}\|$ [17, Def. 2.39]. The corresponding distribution function is the nearest-neighbor distance distribution function, denoted by G^x , which is the cdf of $\|x - \Phi \setminus \{x\}\|$:

$$\begin{aligned} G^x(r) &\triangleq \mathbb{P}^x(\|x - \Phi \setminus \{x\}\| \leq r) \\ &= \mathbb{P}^{!x}(\Phi(b(x, r)) > 0), \end{aligned} \quad (33)$$

where \mathbb{P}^x and $\mathbb{P}^{!x}$ are the Palm and reduced Palm measures (at x). If Φ is stationary, G^x does not depend on the location x and is given by $G(r) = \mathbb{P}^{!o}(\Phi(b(o, r)) > 0)$. Upper and lower bounds on the cdf of the nearest-neighbor distance for the PDP are derived in the following theorem.

Theorem 4. *Let*

$$\begin{aligned} \hat{G}(r) &\triangleq 1 - \frac{1}{P_p(R)} \int_0^R 2\pi\beta t \exp\left(-\beta\pi t^2 - \lambda_I \tilde{A}(R, r, t)\right. \\ &\quad \left.- 2\pi\beta \int_t^\infty (1 - e^{-\lambda_I \tilde{A}(R, r, x)}) x dx\right) dt, \end{aligned} \quad (34)$$

$$\check{G}(r) \triangleq 1 - \frac{1}{P_p(R)} \int_0^R 2\pi\beta t e^{-\beta\pi t^2 - \lambda_I \tilde{A}(R, r, t)} dt. \quad (35)$$

The cdf of the nearest-neighbor distance for the PDP is bounded by $\check{G}(r) < G(r) < \hat{G}(r)$.

Proof: According to (33), the nearest-neighbor distance distribution function of Φ_p is expressed as

$$\begin{aligned} G(r) &= 1 - \mathbb{P}^{!o}(\Phi_p(b(o, r)) > 0) \\ &= 1 - \mathbb{E}^{!o}\left(\prod_{x \in \Phi_p} [1 - \mathbf{1}(\|x\| \leq r)]\right) \\ &= 1 - \mathcal{G}^! [1 - \mathbf{1}(\|x\| \leq r)]. \end{aligned} \quad (36)$$

Following the results in Theorem 2, the upper and lower bounds of $G(r)$ are obtained. Specifically, the upper bound is given by

$$\begin{aligned} G(r) &< 1 - \check{\mathcal{G}}^! [1 - \mathbf{1}(\|x\| \leq r)] \\ &= 1 - \frac{1}{P_p(R)} \int_{b(o, R)} \beta e^{-\beta\pi\|x\|^2 - \lambda_I \int_{b(x, R)} \mathbf{1}(\|z\| \leq r) dz} \\ &\quad \times \exp\left(-\beta \int_{b^c(o, \|x\|)} 1 - e^{-\lambda_I \int_{b(y, R)} \mathbf{1}(\|z\| \leq r) dz} dy\right) dx \\ &= 1 - \frac{1}{P_p(R)} \int_0^R 2\pi\beta t e^{-\beta\pi t^2} e^{-\lambda_I \tilde{A}(R, r, t)} \\ &\quad \times \exp\left(-2\pi\beta \int_t^\infty (1 - e^{-\lambda_I \tilde{A}(R, r, x)}) x dx\right) dt, \end{aligned} \quad (37)$$

and the lower bound is given by

$$G(r) > 1 - \hat{\mathcal{G}}^! [1 - \mathbf{1}(\|x\| \leq r)]$$

$$\begin{aligned}
&= \frac{1}{P_p(R)} \int_{b(o,R)} \beta e^{-\beta\pi\|y\|^2 - \lambda_1 \int_{b(x,R)} \mathbf{1}(\|z\| \leq r) dz} dy \\
&= 1 - \frac{1}{P_p(R)} \int_0^R 2\pi\beta t e^{-\beta\pi t^2 - \lambda_1 \tilde{A}(R,r,t)} dt. \quad (38)
\end{aligned}$$

Since the range of the outer integral in (34) is $[0, R]$, setting $t = R$ as the lower limit of the inner integral yields a lower bound on $\hat{G}(r)$, and accordingly, a simple approximation to the nearest-neighbor distance distribution function is given by

$$\begin{aligned}
G(r) &\approx 1 - \frac{1}{P_p(R)} e^{-2\pi\beta \int_R^\infty (1 - e^{-\lambda_1 \tilde{A}(R,r,x)}) dx} \\
&\quad \times \int_0^R 2\pi\beta t e^{-\beta\pi t^2 - \lambda_1 \tilde{A}(R,r,t)} dt. \quad (39)
\end{aligned}$$

This approximation is validated in Section V to provide an excellent match for the nearest-neighbor distance distribution function of the PDP.

IV. TRANSMISSION SUCCESS PROBABILITY OF WIRELESSLY POWERED NETWORKS

In this section, we analyze the information transmission success probability in a wirelessly powered network, accounting for the energy correlation. The information transmission success probability⁴ is a fundamental communication performance metric, defined as the complementary cumulative distribution function (ccdf) of the SIR, i.e., $P(\theta) \triangleq \mathbb{P}(\text{SIR} > \theta)$, where θ is the SIR threshold. We first adopt the PDP to model the spatial configuration of the energized nodes and provide upper and lower bounds on the information transmission success probability. Secondly, we provide two approximations by a homogeneous PPP and a MCP with the same density.

A. PDP-Based Analysis

In this subsection, we provide the information transmission success probability analysis of a wirelessly powered network, where the locations of the transmitters in the communication phase (i.e., the energized RF-powered nodes) are modeled by a PDP. Since the success probability can be derived through the Laplace transform of the interference, we focus on the Laplace transform of the interference for both Type I and Type II next.

1) *Type I*: In this case, the Laplace transform of I is expressed as

$$\begin{aligned}
\mathcal{L}_I(s) &= \mathbb{E} \left[\exp \left(-s \sum_{x \in \Phi_p} \ell(x) h_{x_o} \right) \right] \\
&= \mathbb{E} \left[\prod_{x \in \Phi_p} \frac{1}{1 + s\ell(x)} \right] \\
&\stackrel{(a)}{=} \mathcal{G} \left[\frac{1}{1 + s\ell(x)} \right], \quad (40)
\end{aligned}$$

⁴Another important performance metric is the information transmission outage probability $P^o = 1 - P_c P(\theta)$, which is the complement of the success probability.

where step (a) follows from the definition of the PGFL. According to the bounds on the PGFL of the PDP derived in Theorem 1, we can also give bounds on the Laplace transform of I as follows. Let $\tilde{\mathcal{L}}_I(s)$ and $\hat{\mathcal{L}}_I(s)$ be a lower bound and upper bound of $\mathcal{L}_I(s)$, respectively. Using polar coordinates, we have

$$\begin{aligned}
\tilde{\mathcal{L}}_I(s) &= \tilde{\mathcal{G}} \left[\frac{1}{1 + s\ell(x)} \right] \\
&= \exp \left(-2\pi\lambda_f \int_0^\infty \left(1 - e^{-\lambda_d \gamma(v,R,s)} \right) v dv \right), \quad (41) \\
\hat{\mathcal{L}}_I(s) &= \hat{\mathcal{G}} \left[\frac{1}{1 + s\ell(x)} \right] \\
&= 2\pi\lambda_f \int_0^\infty e^{-\lambda_f \pi v^2 - \lambda_d \gamma(v,R,s)} v dv, \quad (42)
\end{aligned}$$

where

$$\gamma(v, R, s) = \begin{cases} 2 \int_{R-v}^{R+v} \arccos \left(\frac{v^2 + r^2 - R^2}{2vr} \right) \frac{r dr}{1 + s^{-1} r^\alpha} \\ \quad + 2\pi \int_0^{R-v} \frac{r dr}{1 + s^{-1} r^\alpha}, & v \leq R, \\ 2 \int_{v-R}^{R+v} \arccos \left(\frac{v^2 + r^2 - R^2}{2vr} \right) \frac{r dr}{1 + s^{-1} r^\alpha}, & v > R. \end{cases} \quad (43)$$

Since the transmission success probability is the Laplace transform of I evaluated at $s = \theta d^\alpha$, i.e., $P_1(\theta) = \mathcal{L}_I(\theta d^\alpha)$, we obtain the upper and lower bounds on the success probability by substituting $s = \theta d^\alpha$ into (41) and (42).

It is worth noting that the success probability necessarily tends to zero for $\theta \rightarrow \infty$ while its upper bound $\hat{\mathcal{L}}_I(\theta d^\alpha)$ tends to $e^{-\lambda_d \pi R^2}$. This indicates that the upper bound on the success probability deviates more from the exact result when θ gets large. This is mainly due to the fact that the upper bound of the PGFL $\hat{\mathcal{G}}[v]$ is obtained by merely considering the points in $\Phi_2 \cap b(y_0, R)$ with $y_0 \in \Phi_1$ the nearest point to the origin, thereby neglecting the contribution from the more distant points in Φ_p . To solve this problem, we further approximate the spatial distribution of the points in $\Phi_2 \setminus b(y_0, R)$ with a PPP with density λ_p , which results in an accurate approximation to the Laplace transform of the interference, given in the following corollary.

Corollary 1. Let $\tilde{\gamma}(v, R, s) = 2\pi \int_{R+v}^\infty \frac{r}{1 + s^{-1} r^\alpha} dr$ and

$$\tilde{\mathcal{L}}_I(s) = 2\pi\lambda_f \int_0^\infty e^{-\lambda_f \pi v^2 - \lambda_d \gamma(v,R,s) - \lambda_p \tilde{\gamma}(v,R,s)} v dv. \quad (44)$$

The Laplace transform of the interference is approximated as $\mathcal{L}_I(s) \approx \tilde{\mathcal{L}}_I(s)$.

Proof: To capture the effect from the interfering nodes outside the disk $b(y_0, R)$, we adopt a PPP denoted by Φ_{out} with density λ_p to approximate the spatial distribution of these nodes. Letting $\Psi_p = \Phi_p \cap b(y_0, R)$ we have

$$\begin{aligned}
\mathcal{L}_I(s) &\approx \mathbb{E} \left[\prod_{x \in \Psi_p} \frac{1}{1 + s\ell(x)} \prod_{x \in \Phi_{\text{out}}} \frac{1}{1 + s\ell(x)} \right] \\
&= 2\pi\lambda_f \int_0^\infty e^{-\lambda_f \pi v^2} v \mathbb{E} \left[\prod_{x \in \Psi_p} \frac{1}{1 + s\ell(x)} \right]
\end{aligned}$$

$$\begin{aligned}
& \times \prod_{x \in \Phi_{\text{out}}} \frac{1}{1 + s\ell(x)} \Big| \|y_0\| = v \Big] dv \\
& = 2\pi\lambda_f \int_0^\infty e^{-\lambda_f \pi v^2} v e^{-\lambda_d \int_{b(y_0, R)}^{1 - \frac{1}{1+s\ell(x)}} dx} \\
& \quad \times e^{-\lambda_p \int_{b^c(y_0, R)}^{1 - \frac{1}{1+s\ell(x)}} dx} dv \\
& \stackrel{(a)}{\approx} 2\pi\lambda_f \int_0^\infty e^{-\lambda_f \pi v^2} v e^{-\lambda_d \int_{b(y_0, R)}^{1 - \frac{1}{1+s\ell(x)}} dx} \\
& \quad \times e^{-\lambda_p \int_{b^c(o, v+R)}^{1 - \frac{1}{1+s\ell(x)}} dx} dv, \tag{45}
\end{aligned}$$

where step (a) follows from the fact $b^c(o, v+R) \subset b^c(y_0, R)$. The final result is obtained by using polar coordinates. ■

2) *Type II*: Because of the stationarity of the PDP, in this case, we condition on the desired transmitter belonging to the PDP and being located at the origin. Hence, this node does not contribute to the interference. Letting $\mathcal{L}_{I^1}(s)$ be the conditional Laplace transform of I^1 , we have

$$\begin{aligned}
\mathcal{L}_{I^1}(s) &= \mathbb{E}^{!o} \left[\prod_{x \in \Phi_p} \frac{1}{1 + s\ell(x-z)} \right] \\
&= \mathcal{G}^! \left[\frac{1}{1 + s\ell(x-z)} \right]. \tag{46}
\end{aligned}$$

In the bipolar communication model, since the distance d between a transmitter-receiver pair is usually set relatively small (i.e., $d \ll \lambda_p^{-1/2}$) to avoid many low-reliability links, we approximate $I^1(z)$ with $I^1(o)$, resulting in $\mathcal{L}_{I^1}(s) \approx \mathcal{G}^! \left[\frac{1}{1+s\ell(x)} \right]$. Under this approximation, expressions for the lower and upper bounds on $\mathcal{L}_{I^1}(s)$ can be significantly simplified as follows.

Let $\tilde{\mathcal{L}}_{I^1}(s)$ and $\hat{\mathcal{L}}_{I^1}(s)$ be a lower and upper bounds on $\mathcal{L}_{I^1}(s)$, respectively. Using polar coordinates, we have

$$\begin{aligned}
\tilde{\mathcal{L}}_{I^1}(s) &\approx \check{\mathcal{G}}^! \left[\frac{1}{1 + s\ell(x)} \right] \\
&\stackrel{(b)}{\approx} \frac{2\pi\lambda_f \int_0^R e^{-\lambda_f \pi v^2 - \lambda_d \gamma(v, R, s)} v dv}{P_p(R)} \\
&\quad \times \exp \left(-2\pi\lambda_f \int_R^\infty (1 - e^{-\lambda_d \gamma(v, R, s)}) v dv \right), \tag{47}
\end{aligned}$$

$$\begin{aligned}
\hat{\mathcal{L}}_{I^1}(s) &\approx \hat{\mathcal{G}}^! \left[\frac{1}{1 + s\ell(x)} \right] \\
&= \frac{2\pi\lambda_f}{P_p(R)} \int_0^R e^{-\lambda_f \pi v^2 - \lambda_d \gamma(v, R, s)} v dv, \tag{48}
\end{aligned}$$

where step (b) is obtained using the simplified approximation in (25).

It should be noted that as d gets larger, the impact of the condition that the typical transmitter belongs to the PDP on I^1 gradually diminishes, and accordingly, I^1 tends to have the same statistics as the interference in Type I.

Similar to Type I, we further obtain an approximation of $\mathcal{L}_{I^1}(s)$ based on its upper bound by considering the distant interferers outside the closest disk to the origin, and the following corollary gives the explicit result.

Corollary 2. *Letting*

$$\tilde{\mathcal{L}}_{I^1}(s) \triangleq \frac{2\pi\lambda_f}{P_p(R)} \int_0^R e^{-\lambda_f \pi v^2 - \lambda_d \gamma(v, R, s) - \lambda_p \tilde{\gamma}(v, R, s)} v dv, \tag{49}$$

the Laplace transform of the interference is approximated as $\mathcal{L}_{I^1}(s) \approx \tilde{\mathcal{L}}_{I^1}(s)$.

Although the PDP-based analysis involves two nested integrals, it can be efficiently calculated by using numerical methods since the integrand in the Laplace transform of the interference essentially decreases exponentially with the integration variable.

B. Approximation with PPP

Due to the energy correlation, an exact calculation of the success probability of the typical receiver in a wirelessly powered network seems unfeasible. The approximate expressions for the more realistic model can be traded off against exact ones for a less realistic one, namely the Poisson model, where the spatial distribution of the energized RF-powered nodes is approximated by a homogeneous PPP with the same density. From Slivnyak's theorem [17], conditioning on a point at the origin does not change the distribution of the rest of the process, i.e., the reduced Palm distribution is the same as the distribution of the original PPP. Hence, in the PPP-based approximation, the Laplace transforms of the interference for Types I and II are the same and given by

$$\begin{aligned}
\mathcal{L}_{I_{\text{PPP}}}(s) &= \exp \left(-\lambda_e \int_{\mathbb{R}^2} \frac{1}{1 + s^{-1}\ell^{-1}(x)} dx \right) \\
&= \exp \left(-\lambda_e \pi \frac{\pi\delta}{\sin(\pi\delta)} s^\delta \right), \tag{50}
\end{aligned}$$

and the resulting success probability with the PPP approximation is

$$P(\theta) = \exp \left(-\lambda_e \frac{\pi^2 \delta}{\sin(\pi\delta)} d^2 \theta^\delta \right). \tag{51}$$

Remark 4: The PPP approximation yields the most tractable analytical results for the wirelessly powered networks but leads to the largest deviation from the exact results due to the neglect of the energy correlation.

C. Approximation with MCP

As discussed above, there are some similarities between a PDP and a MCP. Thus, by setting $\lambda = \lambda_f$, $D = R$, and matching the density $\lambda_p = \lambda_c$, we provide another approximation for the performance analysis with an MCP as follows. The interference in a PDP-based network can be approximated by the one in a Poisson cluster network. According to [28, Eq. (34)], the Laplace transforms of the interference for Types I and II are

$$\mathcal{L}_{I_{\text{PCP}}}(s) = \exp \left\{ -\lambda \int_{\mathbb{R}^2} [1 - \exp(-\bar{c}\nu(s, y, z))] dy \right\} \tag{52}$$

$$\mathcal{L}_{I_{\text{PCP}}^!}(s) = \mathcal{L}_{I_{\text{PCP}}}(s) \int_{\mathbb{R}^2} \exp(-\bar{c}\nu(s, y, z)) f(y) dy, \tag{53}$$

where

$$\nu(s, y, z) = \int_{\mathbb{R}^2} \frac{f(x)}{1 + (s\ell(x - y - z))^{-1}} dx, \tag{54}$$

and $f(x)$ is the probability density function of the node distribution around the parent point. For the MCP, we have

$$f(x) = \frac{1}{\pi R^2} \mathbf{1}(x \in b(o, R)). \tag{55}$$

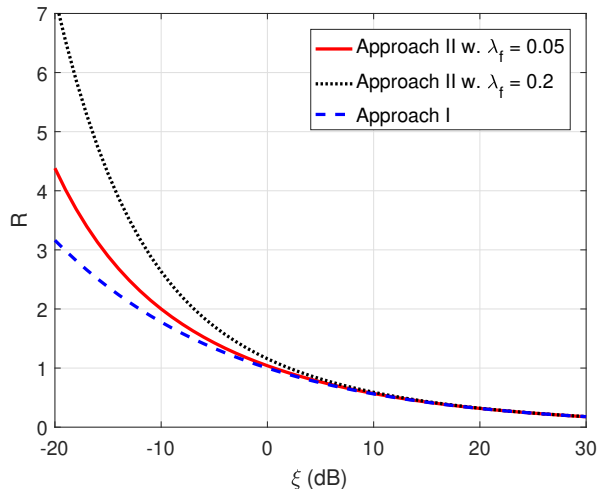


Fig. 3. The relationship between R in the PDP and ξ in the EPP for different approaches.

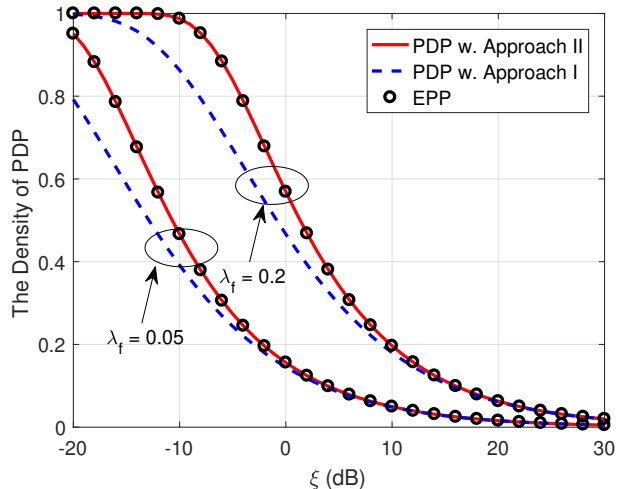


Fig. 4. The density of the PDP versus ξ in the EPP for different approaches.

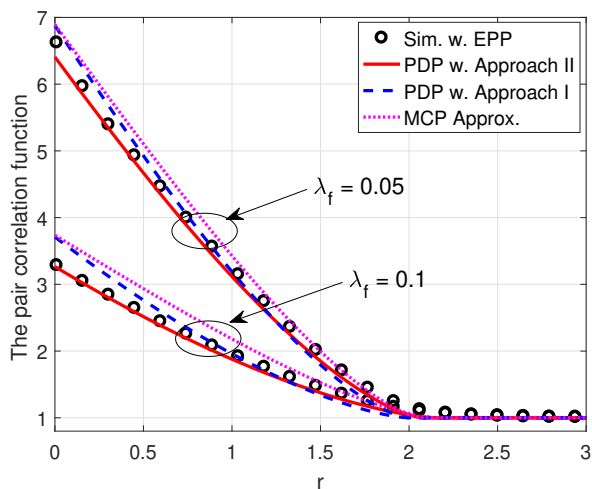


Fig. 5. The comparison of pcfs for different options with different λ_f .

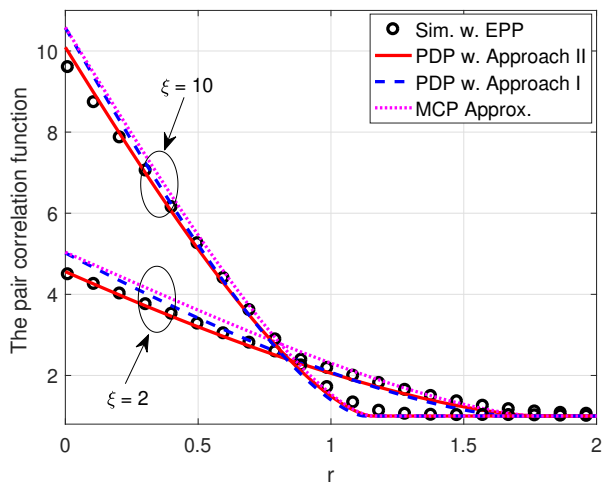


Fig. 6. The comparison of pcfs for different options with different ξ .

Remark 5: Despite the accuracy of the approximation provided by the MCP, the resulting expressions for performance metrics are more complicated compared to the PDP-based analysis and the PPP-based approximation. In addition, the MCP approximation may still be not accurate beyond a specific range of system parameters. After all, the higher-order statistics are also ignored.

V. NUMERICAL RESULTS

In this section, we provide numerical results for the properties of the PDP and the performance of PDP-modeled wirelessly powered communication networks. The default values of the main parameters are $\beta = \lambda_f = 0.1$, $\lambda_l = \lambda_d = 1$, $\alpha = 4$, $\xi = 1$, and $d = 0.1$ where applicable.

A. Basic Properties of the PDP

Figure 3 shows how the key parameter R changes with the energy threshold ξ when the PDP is adopted to characterize the EPP via the proposed two different approaches. We observe

that the disk radius R in the PDP decreases with increasing ξ , and the curves for different approaches and RF transmitter densities tend to be consistent with each other when ξ is larger than a certain value, about 10 dB. For a given ξ , the value of R obtained by Approach I is smaller than that by Approach II, because the former is based on a sufficient condition such that $\lambda_p < \lambda_e$ while the latter guarantees $\lambda_p = \lambda_e$. Furthermore, for a relatively sparse energy harvesting network (i.e., a smaller density of RF transmitters), the disk radius also gets smaller in Approach II. However, in Approach I, the disk radius is independent of λ_f . Thus, while Approach I is relatively simple, its accuracy for approaching the PDP to the EPP is inferior to that of Approach II.

Figure 4 shows the relationship between the density λ_p of the PDP and the energy threshold ξ in the EPP for different λ_f after determining the value of R via the two approaches. Similar to Figure 3, the gap between the curves of Approaches I and II gradually decreases and finally tends to zero as ξ increases. Besides, the behaviors of R and λ_p as a function of λ_f are the same. Since the energy correlation is stronger

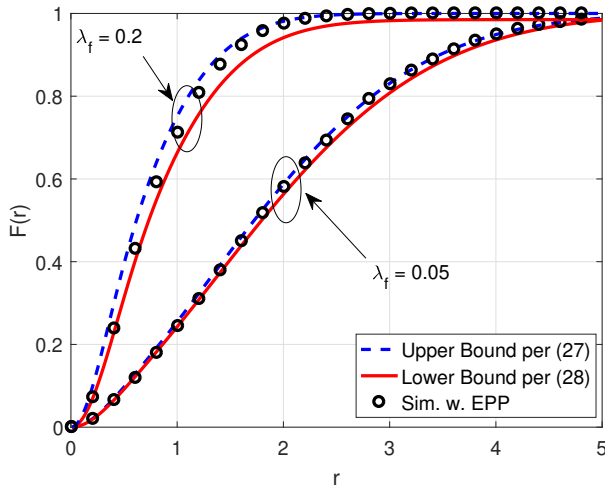


Fig. 7. The contact distribution functions of the PDP with different λ_f .

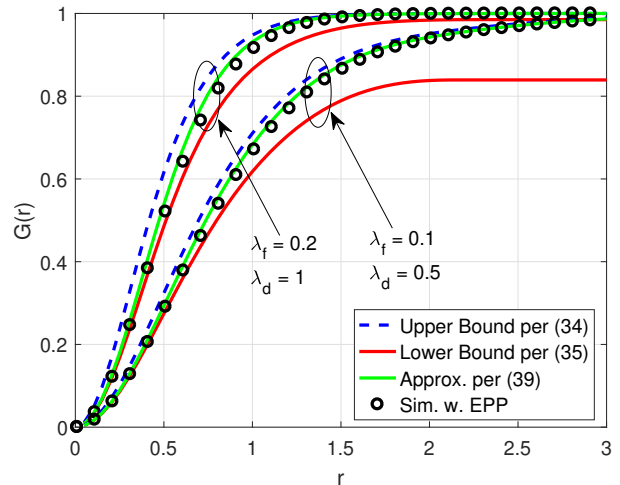


Fig. 8. The nearest-neighbor distribution functions of the PDP with different λ_f .

in a sparser energy harvesting network, the disk radius in the case with a smaller density of RF transmitter is smaller, thus resulting in a smaller density of the active RF-powered nodes.

Figures 5 and 6 compare the pcfs of different point processes for different RF transmitter densities and energy thresholds, where the one of the EPP is obtained via simulation using the **spatstat library** in the **R language** and the one of the PDP is obtained analytically according to (15) in Section III-A. For the MCP, the pcf is [17, Section 6.4]

$$g_M(r) = 1 + \frac{1}{\lambda} \frac{A(D, r)}{\pi^2 D^4}, \quad (56)$$

where $\lambda = \lambda_f$, $D = R$ and $\lambda_p = \lambda \bar{c}$. It can be observed that while the PDP and the MCP provide excellent approximations to the EPP in terms of the pcf, the Approach II-based PDP performs best for different parameter setups. An important observation is that all the pcfs are larger than in the PPP case, indicating the positive energy correlation (clustering behavior) among the active RF-powered nodes. Furthermore, we observe that a smaller density of RF transmitters or a larger energy threshold leads to stronger clustering, which means the clustering behavior is increasingly prominent as the RF transmitters become sparse or the required amount of energy increases (i.e., fewer RF-powered nodes are retained).

Figure 7 plots the bounds on the contact distribution functions of the PDP in comparison with that of the EPP. It validates the accuracy of the PDP in modeling the energized RF-powered nodes and demonstrates the tightness of the derived bounds.

Figure 8 plots the bounds on the nearest-neighbor distribution functions of the PDP in comparison with that of the EPP. Here the lower bound is relatively loose in the case of $\lambda_f = 0.1$ and $\lambda_d = 0.5$. Such deviation occurs when there is no other point in the closest disk to the origin. In contrast, the proposed approximation, simpler than the bounds, is extremely close to the simulation result.

B. Information Transmission Success Probability

Figure 9 compares the transmission success probability in the communication phase using different approaches for Types I and II, where the simulation result is based on a given EPP incorporating practical energy harvesting factors. We observe that for both types of success probabilities, the proposed lower bound and the approximation by the PDP are quite close to the simulation results, demonstrating the effectiveness and rationality of using the PDP to characterize the EPP. While the upper bound deviates from the actual result in Type I, it provides a good approximation to that in Type II. It can be also seen that the PPP-based results always deviate significantly from the simulations while the MCP-based results provide the best approximation in terms of both types of success probabilities. A key observation is that the PPP-based curve is the same in both types of scenarios, and in particular, it is pessimistic for Type I but optimistic (with larger deviations) for Type II. In Type I, we focus on the interference from all nodes in a point process to the origin. Obviously, the node density of the PPP is larger than the disk/cluster density in a PDP or MCP, hence the probability of having a strong interferer nearby in the PPP case is higher than in the other cases. In contrast, in Type II, we focus on the interference at a node belonging to this point process suffered by all the other nodes. In this case, the probability that there is a strong interferer nearby in the PDP or MCP case is much higher than in the PPP case, since points in these point processes exhibit clustering. In other words, the positive energy correlation has a more important effect on the Type II communication performance.

Figure 10 compares the EPP-based simulations and the PDP-based analytical results for two types of success probabilities with different RF transmitter densities and energy thresholds. It is observed that the PDP-based approximation matches with the actual result extremely well for different parameter setups since it incorporates both strong interferers nearby and the weak ones far away. The lower bound is tight for certain parameter settings, e.g., for a small density of RF

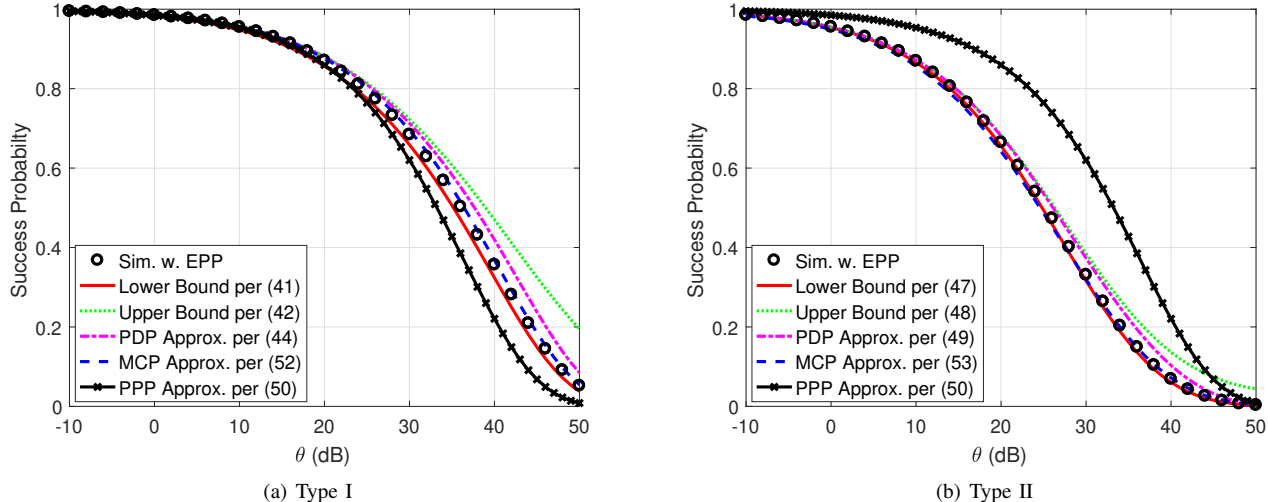


Fig. 9. The comparison of different approaches for the transmission success probability analysis.

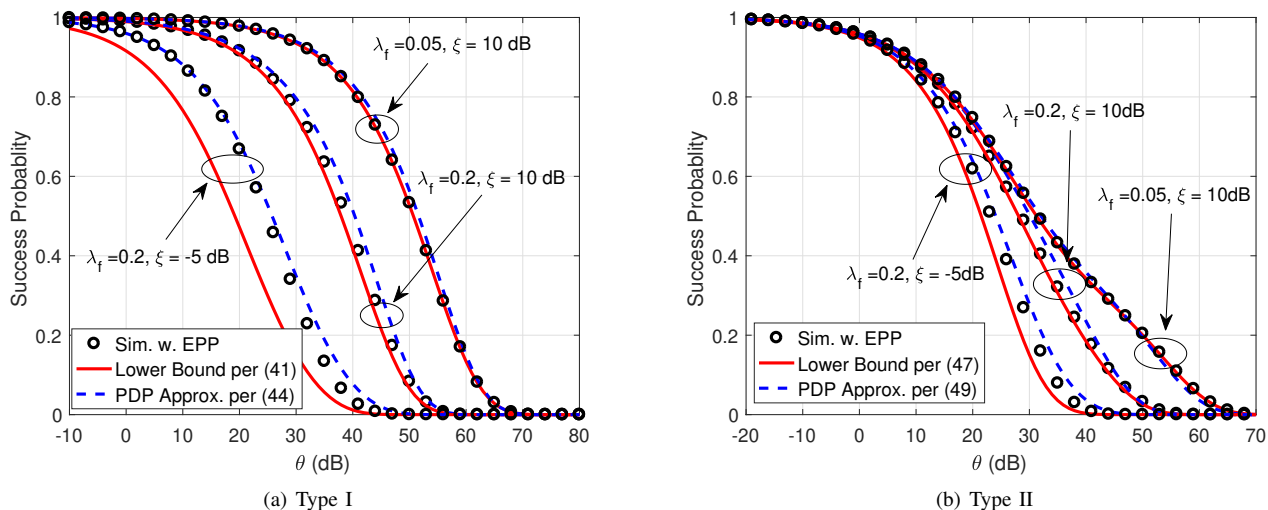


Fig. 10. The success probability for the PDP-based network with different λ_f and ξ .

transmitters (sparse deployment) or a large energy threshold (strong clustering behavior). The reason is that the overlaps among different disks are ignored in the PDP model, and the larger λ_f or the smaller ξ (leading to a larger R), the more likely the overlaps occur.

VI. CONCLUSIONS

Since the energy correlation establishes a dependence between energy and information transfer, it plays an important role in the communication phase. Although some prior work has addressed the energy correlation issue, an exact characterization of the communication performance is still unavailable. To address this, we propose a tractable yet accurate model, named PDP, for the energized RF-powered nodes and focus on the accurate performance characterization of a wirelessly powered network with energy correlation. The PDP can be viewed as a kind of EPP but with a simpler structure, which

is fully characterized by its first- and second-order statistics. We provided tight bounds and accurate approximations for its PGFL, contact distribution function as well as nearest-neighbor distance distribution function, respectively. Hence, the Laplace transform of the interference and the information transmission success probability in wirelessly powered networks can be characterized. As the energy correlation is considered, the resulting performance reflects the impact of the energy harvesting on the communication phase more accurately than the previous one based on the independence assumption.

The key insight is that the PDP model lies in between the PPP and MCP, achieving an excellent balance between accuracy and tractability. The PPP approximation leads to closed-form results that deviate strongly from the exact results, as it ignores the energy correlation. While the MCP approximation is mostly accurate, its analytical expressions have the most

complicated form (four-level integrals). In contrast, the PDP model achieves almost the same accuracy in a much simpler form (two-level integrals). Moreover, it should be noted that the work in this paper is not limited to the performance analysis of wirelessly powered networks but has applications in a variety of wireless networks where the network topology is modeled by a PDP.

APPENDIX A PROOF OF LEMMA 1

Proof: According to the definition of Ripley's K function [17, Def. 6.8], we have

$$\lambda_p K(r) = \frac{2\pi}{\lambda_p} \int_0^r \rho_{\text{mi}}^{(2)}(u) u du, \quad (57)$$

where $\lambda_p K(r)$ is the mean number of points $y \in \Phi_p$ that satisfy $0 \leq \|y - x\| \leq r$ given that $x \in \Phi_p$. Hence we have

$$\begin{aligned} & \lambda_p K(r) \\ &= \mathbb{E}^{!o}[\Phi_p(b(o, r))] \\ &= \mathbb{E} \left[\sum_{y \in \Phi_2} \mathbf{1}(\|y\| < r \cap \Phi_1(b(y, R)) > 0) \mid \Phi_1(b(o, R)) > 0 \right] \\ &\stackrel{(a)}{=} \lambda_I \int_{b(o, r)} \mathbb{P}(\Phi_1(b(y, R)) > 0 \mid \Phi_1(b(o, R)) > 0) dy \\ &= \frac{\lambda_I^2}{\lambda_p} \int_{b(o, r)} \mathbb{P}(\Phi_1(b(y, R)) > 0, \Phi_1(b(o, R)) > 0) dy, \quad (58) \end{aligned}$$

where step (a) uses Campbell's theorem. Letting $u \triangleq \|y\|$, $V_u(R) \triangleq b(o, R) \cap b(y, R)$ and $b^c(y, R) \triangleq b(y, R) \setminus V_u(R)$, the event $\{\Phi_1(b(y, R)) > 0, \Phi_1(b(o, R)) > 0\}$ is partitioned into two events: one is $\{\Phi_1(V_u(R)) > 0\}$; the other is $\{\Phi_1(b^c(o, R)) > 0, \Phi_1(b^c(y, R)) > 0\}$ conditioning on $\{\Phi_1(V_u(R)) = 0\}$. According to the total probability law and polar coordinates, we have

$$\begin{aligned} \lambda_p K(r) &= \frac{2\pi\lambda_I^2}{\lambda_p} \int_0^r \left(1 - 2e^{-\beta\pi R^2} \right. \\ &\quad \left. + e^{-\beta(2\pi R^2 - A(R, u))} \right) u du. \quad (59) \end{aligned}$$

Comparing (58) and (59), the final result is obtained. \blacksquare

APPENDIX B PROOF OF THEOREM 1

Proof: According to the definition the Boolean model, we have

$$\begin{aligned} \mathcal{G}[v] &= \mathbb{E} \left(\prod_{x \in \Phi_2 \cap \Xi} v(x) \right) \\ &\stackrel{(a)}{>} \mathbb{E} \left(\prod_{y \in \Phi_1} \prod_{x \in \Phi_2 \cap b(y, R)} v(x) \right) \\ &= \mathbb{E}_{\Phi_1} \left[\prod_{y \in \Phi_1} \exp \left(-\lambda_I \int_{b(y, R)} 1 - v(x) dx \right) \right] \\ &= \exp \left(-\beta \int_{\mathbb{R}^2} 1 - e^{-\lambda_I V(R, y)} dy \right), \quad (60) \end{aligned}$$

where step (a) follows from $\Phi_2 \cap \Xi \subset \bigcup_{y \in \Phi_1} \{\Phi_2 \cap b(y, R)\}$ and $V(R, y) = \int_{b(y, R)} [1 - v(x)] dx$. Since $\Phi_2 \cap b(y_0, R) \subset \Phi_2 \cap \Xi$, we have

$$\begin{aligned} \mathcal{G}[v] &< \mathbb{E} \left(\prod_{x \in \Phi_2 \cap b(y_0, R)} v(x) \right) \\ &= \mathbb{E}_{y_0} \left[\exp \left(-\lambda_I \int_{b(y_0, R)} 1 - v(x) dx \right) \right] \\ &= \int_0^\infty \int_0^{2\pi} \frac{1}{2\pi} f_{\|y_0\|}(t) e^{-\lambda_I V(R, y_0)} \Big|_{y_0=t(\cos \psi, \sin \psi)} dt d\psi \\ &= \int_0^\infty \int_0^{2\pi} \beta t e^{-\beta\pi t^2 - \lambda_I V(R, y_0)} \Big|_{y_0=t(\cos \psi, \sin \psi)} dt d\psi \\ &= \beta \int_{\mathbb{R}^2} e^{-\beta\pi \|y\|^2 - \lambda_I V(R, y)} dy. \quad (61) \end{aligned}$$

\blacksquare

APPENDIX C PROOF OF THEOREM 2

Proof: According to the definition of the Boolean model, we have

$$\begin{aligned} \mathcal{G}^! [v] &= \mathbb{E}^{!o} \left(\prod_{x \in \Phi_p} v(x) \right) \\ &= \mathbb{E}^{!o} \left[\prod_{x \in \Phi_2 \cap \Xi} v(x) \mid \Phi_1(b(o, R)) > 0 \right] \\ &> \mathbb{E}^{!o} \left(\prod_{y \in \Phi_1} \prod_{x \in \Phi_2 \cap b(y, R) \setminus \{o\}} v(x) \mid \Phi_1(b(o, R)) > 0 \right) \\ &= \mathbb{E}_{\Phi_1} \left[\prod_{y \in \Phi_1} \mathbb{E}_{\Phi_2}^{!o} \left(\prod_{x \in \Phi_2 \cap b(y, R)} v(x) \right) \mid \Phi_1(b(o, R)) > 0 \right] \\ &\stackrel{(a)}{=} \mathbb{E}_{\Phi_1} \left[\prod_{y \in \Phi_1} \mathbb{E}_{\Phi_2} \left(\prod_{x \in \Phi_2 \cap b(y, R)} v(x) \right) \mid \|y_0\| < R \right] \\ &= \mathbb{E}_{\Phi_1} \left[\prod_{y \in \Phi_1} e^{-\lambda_I V(R, y)} \mid \|y_0\| < R \right] \\ &= \mathbb{E}_{\Phi_1} \left[e^{-\lambda_I V(R, y_0)} \prod_{y \in \Phi_1 \setminus \{y_0\}} e^{-\lambda_I V(R, y)} \mid \|y_0\| < R \right] \\ &\stackrel{(b)}{=} \int_0^{2\pi} \int_0^R \frac{\tilde{f}(t)}{2\pi} e^{-\lambda_I V(R, y_0)} \Big|_{y_0=t(\cos \psi, t \sin \psi)} \\ &\quad \times \exp \left(-\beta \int_{b^c(o, t)} 1 - e^{-\lambda_I V(R, y)} dy \right) dt d\psi \\ &= \int_{b(o, R)} \frac{\beta e^{-\beta\pi \|x\|^2 - \lambda_I V(R, x)}}{P_p(R)} \\ &\quad \times \exp \left(-\beta \int_{b^c(o, \|x\|)} 1 - e^{-\lambda_I V(R, y)} dy \right) dx, \quad (62) \end{aligned}$$

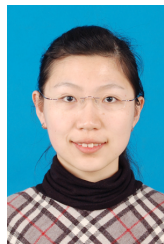
where step (a) follows from Slivnyak's theorem applied to Φ_2 and $b^c(o, t) = \mathbb{R}^2 \setminus b(o, t)$ and step (b) follows that $\tilde{f}(t) = \frac{2\pi\beta t e^{-\beta\pi t^2}}{P_p(R)}$ is the conditional probability density function of $\|y_0\|$ given $\|y_0\| < R$. Since $\Phi_2 \cap b(y_0, R) \subset \Phi_2 \cap \Xi$, we have

$$\mathcal{G}^! [v] < \mathbb{E}^{!o} \left(\prod_{x \in \Phi_2 \cap b(y_0, R)} v(x) \mid \Phi_1(b(o, R)) > 0 \right)$$

$$\begin{aligned}
&= \mathbb{E}_{y_0} \left[\mathbb{E}_{\Phi_2} \left(\prod_{x \in \Phi_2 \cap b(y_0, R)} v(x) \right) \mid \|y_0\| < R \right] \\
&= \mathbb{E}_{y_0} \left[e^{-\lambda_1 V(R, y_0)} \mid \|y_0\| < R \right] \\
&= \int_0^\infty \int_0^{2\pi} \frac{\tilde{f}(t)}{2\pi} e^{-\lambda_1 V(R, y_0)} \Big|_{y_0=t(\cos \psi, \sin \psi)} dt d\psi \\
&= \int_{b(o, R)} \frac{\beta e^{-\beta\pi\|y\|^2 - \lambda_1 V(R, y)}}{P_p(R)} dy. \tag{63}
\end{aligned}$$

REFERENCES

- [1] N. Deng and M. Haenggi, "Success probability in wirelessly powered networks with energy correlation," in *IEEE International Conference on Communications (ICC'2020)*, Dublin, Ireland, Jun. 2020.
- [2] K. Huang and X. Zhou, "Cutting the last wires for mobile communications by microwave power transfer," *IEEE Communications Magazine*, vol. 53, no. 6, pp. 86–93, Jun. 2015.
- [3] S. Bi, C. K. Ho, and R. Zhang, "Wireless powered communication: opportunities and challenges," *IEEE Communications Magazine*, vol. 53, no. 4, pp. 117–125, Apr. 2015.
- [4] M. Haenggi, J. Andrews, F. Baccelli, O. Dousse, and M. Franceschetti, "Stochastic geometry and random graphs for the analysis and design of wireless networks," *IEEE Journal on Selected Areas in Communications*, vol. 27, no. 7, pp. 1029–1046, Sept. 2009.
- [5] K. Huang and V. K. N. Lau, "Enabling wireless power transfer in cellular networks: Architecture, modeling and deployment," *IEEE Transactions on Wireless Communications*, vol. 13, no. 2, pp. 902–912, Feb. 2014.
- [6] A. H. Sakr and E. Hossain, "Analysis of K -tier uplink cellular networks with ambient RF energy harvesting," *IEEE Journal on Selected Areas in Communications*, vol. 33, no. 10, pp. 2226–2238, Oct. 2015.
- [7] M. Di Renzo and W. Lu, "System-level analysis and optimization of cellular networks with simultaneous wireless information and power transfer: Stochastic geometry modeling," *IEEE Transactions on Vehicular Technology*, vol. 66, no. 3, pp. 2251–2275, Mar. 2017.
- [8] N. Deng and M. Haenggi, "The energy and rate meta distributions in wirelessly powered D2D networks," *IEEE Journal on Selected Areas in Communications*, vol. 37, no. 2, pp. 269–282, Feb. 2019.
- [9] I. Krikidis, "Simultaneous information and energy transfer in large-scale networks with/without relaying," *IEEE Transactions on Communications*, vol. 62, no. 3, pp. 900–912, Mar. 2014.
- [10] S. Lee, R. Zhang, and K. Huang, "Opportunistic wireless energy harvesting in cognitive radio networks," *IEEE Transactions on Wireless Communications*, vol. 12, no. 9, pp. 4788–4799, Sept. 2013.
- [11] Y. Liu, L. Wang, S. A. R. Zaidi, M. Elkashlan, and T. Q. Duong, "Secure D2D communication in large-scale cognitive cellular networks: A wireless power transfer model," *IEEE Transactions on Communications*, vol. 64, no. 1, pp. 329–342, Jan. 2016.
- [12] L. Shi, L. Zhao, K. Liang, and H. Chen, "Wireless energy transfer enabled D2D in underlying cellular networks," *IEEE Transactions on Vehicular Technology*, vol. 67, no. 2, pp. 1845–1849, Feb. 2018.
- [13] X. Zhou, J. Guo, S. Durrani, and M. Di Renzo, "Power beacon-assisted millimeter wave ad hoc networks," *IEEE Transactions on Communications*, vol. 66, no. 2, pp. 830–844, Feb. 2018.
- [14] T. A. Khan, A. Alkhateeb, and R. W. Heath, "Millimeter wave energy harvesting," *IEEE Transactions on Wireless Communications*, vol. 15, no. 9, pp. 6048–6062, Sept. 2016.
- [15] C. Psomas and I. Krikidis, "Energy beamforming in wireless powered mmWave sensor networks," *IEEE Journal on Selected Areas in Communications*, vol. 37, no. 2, pp. 424–438, Feb. 2019.
- [16] N. Deng and M. Haenggi, "Energy correlation in wirelessly powered networks," in *IEEE International Conference on Communications (ICC'19)*, Shanghai, China, May 2019.
- [17] M. Haenggi, *Stochastic geometry for wireless networks*. Cambridge University Press, 2012.
- [18] X. Lu, I. Flint, D. Niyato, N. Privault, and P. Wang, "Self-sustainable communications with RF energy harvesting: Ginibre point process modeling and analysis," *IEEE Journal on Selected Areas in Communications*, vol. 34, no. 5, pp. 1518–1535, May 2016.
- [19] H. Kong, P. Wang, D. Niyato, and Y. Cheng, "Modeling and analysis of wireless sensor networks with/without energy harvesting using Ginibre point processes," *IEEE Transactions on Wireless Communications*, vol. 16, no. 6, pp. 3700–3713, Jun. 2017.
- [20] M. A. Kishk and H. S. Dhillon, "Coexistence of RF-powered IoT and a primary wireless network with secrecy guard zones," *IEEE Transactions on Wireless Communications*, vol. 17, no. 3, pp. 1460–1473, Mar. 2018.
- [21] K. Han and K. Huang, "Wirelessly powered backscatter communication networks: Modeling, coverage, and capacity," *IEEE Transactions on Wireless Communications*, vol. 16, no. 4, pp. 2548–2561, Apr. 2017.
- [22] L. Chen, W. Wang, and C. Zhang, "Stochastic wireless powered communication networks with truncated cluster point process," *IEEE Transactions on Vehicular Technology*, vol. 66, no. 12, pp. 11286–11294, Dec. 2017.
- [23] F. Fleischer, C. Gloaguen, H. Schmidt, V. Schmidt, and F. Schweiggert, "Simulation algorithm of typical modulated Poisson-Voronoi cells and application to telecommunication network modelling," *Japan Journal of Industrial & Applied Mathematics*, vol. 25, no. 3, pp. 305–330, 2008.
- [24] R. K. Ganti and M. Haenggi, "Regularity in sensor networks," in *2006 International Zurich Seminar on Communications*. IEEE, 2006, pp. 186–189.
- [25] C. Lee and M. Haenggi, "Interference and outage in Poisson cognitive networks," *IEEE Transactions on Wireless Communications*, vol. 11, no. 4, pp. 1392–1401, Apr. 2012.
- [26] N. Deng, W. Zhou, and M. Haenggi, "Heterogeneous cellular network models with dependence," *IEEE Journal on Selected Areas in Communications*, vol. 33, no. 10, pp. 2167–2181, 2015.
- [27] J. Gil-Pelaez, "Note on the inversion theorem," *Biometrika*, vol. 38, pp. 481–482, Dec. 1951.
- [28] R. Ganti and M. Haenggi, "Interference and outage in clustered wireless ad hoc networks," *IEEE Transactions on Information Theory*, vol. 55, no. 9, pp. 4067–4086, 2009.



Na Deng (S'12-M'17) received the B.S. and Ph.D. degrees in information and communication engineering from the University of Science and Technology of China (USTC), Hefei, China, in 2010 and 2015, respectively. Currently she is an Associate Professor at Dalian University of Technology, Dalian, China. In 2013–2014, she was a Visiting Student in Prof. Martin Haenggi's group at the University of Notre Dame, Notre Dame, IN, USA, and in 2015–2016 she was a Senior Engineer at Huawei Technologies Co., Ltd., Shanghai, China. Her scientific interests

include networking and wireless communications, green communications, and network design based on wireless big data.



Martin Haenggi (S'95-M'99-SM'04-F'14) received the Dipl.-Ing. (M.Sc.) and Dr.sc.techn. (Ph.D.) degrees in electrical engineering from the Swiss Federal Institute of Technology in Zurich (ETH) in 1995 and 1999, respectively. Currently he is the Freimann Professor of Electrical Engineering and a Concurrent Professor of Applied and Computational Mathematics and Statistics at the University of Notre Dame, Indiana, USA. In 2007-2008, he was a visiting professor at the University of California at San Diego, and in 2014-2015 he was an Invited Professor

at EPFL, Switzerland. He is a co-author of the monographs "Interference in Large Wireless Network" (NOW Publishers, 2009) and "Stochastic Geometry Analysis of Cellular Networks" (Cambridge University Press, 2018) and the author of the textbook "Stochastic Geometry for Wireless Networks" (Cambridge, 2012), and he published 16 single-author journal articles. His scientific interests lie in networking and wireless communications, with

an emphasis on cellular, amorphous, ad hoc (including D2D and M2M), cognitive, and vehicular networks. He served as an Associate Editor of the Elsevier Journal of Ad Hoc Networks, the IEEE Transactions on Mobile Computing (TMC), the ACM Transactions on Sensor Networks, as a Guest Editor for the IEEE Journal on Selected Areas in Communications, the IEEE Transactions on Vehicular Technology, and the EURASIP Journal on Wireless Communications and Networking, as a Steering Committee member of the TMC, and as the Chair of the Executive Editorial Committee of the IEEE Transactions on Wireless Communications (TWC). From 2017 to 2018, he was the Editor-in-Chief of the TWC. Currently he is an editor for MDPI Information. For both his M.Sc. and Ph.D. theses, he was awarded the ETH medal. He also received a CAREER award from the U.S. National Science Foundation in 2005 and three awards from the IEEE Communications Society, the 2010 Best Tutorial Paper award, the 2017 Stephen O. Rice Prize paper award, and the 2017 Best Survey paper award, and he is a Clarivate Analytics Highly Cited Researcher.